Ray chaos in underwater acoustics

Kevin B. Smith, Michael G. Brown and Frederick D. Tappert

Citation: The Journal of the Acoustical Society of America **91**, 1939 (1992); doi: 10.1121/1.403677
View online: https://doi.org/10.1121/1.403677
View Table of Contents: https://asa.scitation.org/toc/jas/91/4
Published by the Acoustical Society of America

Ray chaos in underwater acoustics

Kevin B. Smith, Michael G. Brown, and Frederick D. Tappert
Rosenstiel School of Marine and Atmospheric Science, University of Miami, 4600 Rickenbacker Causeway, Miami, Florida 33149

(Received 16 August 1991; accepted for publication 18 December 1991)

Generically, in range-dependent environments, the acoustic wave equation cannot be solved by techniques which require that variables be separated. Under such conditions, the acoustic ray equations, which have Hamiltonian form, are nonintegrable. At least some ray trajectories are expected to exhibit chaotic motion, i.e., extreme sensitivity to initial and environmental conditions. These ideas are illustrated numerically using simple models of the ocean sound channel with weak periodic range dependence. The use of Poincaré sections, power spectra, and Lyapunov exponents to investigate and characterize ray chaos are discussed. The practical importance of chaotic ray trajectories—a limitation on one's ability to make deterministic predictions using ray theory—is emphasized.

PACS numbers: 43.30.Cq, 43.30.Ft, 43.25.Rq

INTRODUCTION

When the sound speed varies as a function of depth only and the ocean surface and bottom correspond to surfaces of constant depth, the acoustic wave equation can be solved by a variety of techniques which depend on separating variables. Under such conditions, the acoustic ray equations, which have Hamiltonian form, are integrable, and neighboring ray trajectories diverge slowly—according to a power law, on average. In the generic range-dependent problem, however, the ray equations are not integrable and at least some ray trajectories exhibit chaotic behavior. Such rays are characterized by rapid—exponential, on average—divergence from their neighbors. From a practical point of view, chaotic ray trajectories are important because they impose a limitation on one's ability to make deterministic predictions using ray theory.

In this paper, these ideas are explored and illustrated using simple, periodically range-dependent models of the ocean sound channel. We restrict our attention to periodic range dependence for two reasons. First, these simple models serve to illustrate the important differences between regular and chaotic ray motion. Second, the assumption of periodic range dependence allows a particularly simple and insightful geometric device, the Poincaré section, to be used.

The study of ray chaos in underwater acoustics involves the application of results from the study of nonintegrable Hamiltonian systems. This topic is reviewed in the articles by Berry (1977) and Henon (1983) and the books by Lichtenberg and Lieberman (1983), Tabor (1989) and Gutzwiller (1990), among others. The application of these results to sound propagation problems has previously been discussed by Palmer *et al.* (1988), Abdullaev and Zaslavskii (1989), Tappert *et al.* (1991), and Brown *et al.* (1991a and 1991b).

The remainder of this paper is organized as follows. In the next section we discuss three sets of acoustic ray equations, the relationship between these equations, and the connection between integrability of the ray equations and the type of motion, chaotic or regular, exhibited by ray trajectories. In Secs. II and III, we discuss the use of Poincaré sections and power spectra, respectively, to investigate the type of motion exhibited by ray trajectories. In Sec. IV, a quantitative measure of the degree of chaos, the Lyapunov exponent, is discussed. In this context, we introduce the notion of a ray "predictability horizon." In Sec. V, we consider the evolution of a continuum of ray initial conditions, i.e., a fan of rays, and argue that under chaotic conditions the number of eigenrays grows exponentially in range. Our results are summarized in Sec. VI.

I. RAY EQUATIONS, INTEGRABILITY, AND CHAOS

In this section we consider the relationship between three sets of acoustic ray equations—the standard (two-way) elliptic ray equations, the one-way elliptic ray equations, and the parabolic ray equations. All three sets of ray equations are shown to be integrable when the environment is range independent, but are expected to be nonintegrable when the environment is range dependent. Numerical results that are presented later for the one-way elliptic ray equations and the parabolic ray equations are in good qualitative agreement, suggesting that, for the purpose of studying ray chaos in underwater acoustics, use of the parabolic ray equations is justified. Other methods of modeling ray propagation in range-dependent environments are described by Foreman (1983) and Jones *et al.* (1986), for example.

The acoustic ray equations consistent with the elliptic (Helmholtz) wave equation in two space dimensions are (see, e.g., Landau and Lifshitz, 1959)

$$\frac{dz}{dt} = \frac{\partial \omega}{\partial k_z}, \tag{1a}$$

$$\frac{dk_z}{dt} = -\frac{\partial \omega}{\partial z} \tag{1b}$$

and

$$\frac{dr}{dt} = \frac{\partial \omega}{\partial k_r}, \tag{1c}$$

 0001-4966/92/041939-11$00.80

$$\frac{dk_r}{dt} = -\frac{\partial \omega}{\partial r}, \tag{1d}$$

where

$$\omega = ck = c(k_z^2 + k_r^2)^{1/2}. \tag{2}$$

Here, t is time, $\omega = \omega(z,r,k_z,k_r)$ is the angular frequency of the wave, $c = c(z,r)$ is the sound speed, and $\mathbf{k} = (k_z,k_r)$ with $|\mathbf{k}| = k$, is the wave-number vector. Depth and range are denoted by z and r, respectively.

Equations (1) and (2) define an autonomous Hamiltonian system with two degrees of freedom. Here ω acts as the Hamiltonian, z and r are position coordinates, and k_z and k_r are the corresponding momenta. It follows from (1) that ω is constant along any ray trajectory,

$$\frac{d\omega}{dt} = \frac{\partial \omega}{\partial r}\frac{dr}{dt} + \frac{\partial \omega}{\partial z}\frac{dz}{dt} + \frac{\partial \omega}{\partial k_r}\frac{dk_r}{dt} + \frac{\partial \omega}{\partial k_z}\frac{dk_z}{dt} = 0. \tag{3}$$

In other words, ω is a constant of the motion.

Consider first the range-independent problem, $c = c(z)$. It follows from (1d) and (2) that $dk_r/dt = 0$ in this case. Thus k_r is a second constant of the motion. The ray equations (1) are integrable provided the two constants of the motion ω and k_r are independent and are in involution, i.e., their Poisson bracket vanishes (see, e.g., Tabor, 1989). This is indeed the case. To see this, first note that it follows from (2) that

$$k_r = (\omega^2/c^2 - k_z^2)^{1/2}. \tag{4}$$

Then, using (2) and (4) with $c = c(z)$ (so that $\partial\omega/\partial r = \partial k_r/dr = 0$), the Poisson bracket is

$$[\omega,k_r] = \left(\frac{\partial \omega}{\partial z}\frac{\partial k_r}{\partial k_z} - \frac{\partial k_r}{\partial z}\frac{\partial \omega}{\partial k_z}\right) + \left(\frac{\partial \omega}{\partial r}\frac{\partial k_r}{\partial k_r} - \frac{\partial k_r}{\partial r}\frac{\partial \omega}{\partial k_r}\right)$$

$$= \frac{1}{k}\frac{k_z}{k_r}\frac{\partial c}{\partial z}\left(\frac{\omega^2}{c^2} - k^2\right) = 0. \tag{5}$$

Integrability guarantees regular (nonchaotic) motion so in range-independent environments, $c = c(z)$, ray motion is entirely regular.

Now consider the range-dependent problem, $c = c(z,r)$. Again, ω is a constant of the motion. In general, however, no other constant of the motion exists. Furthermore, no general analytic procedure is known for determining whether a second constant of the motion exists. For this reason, this question must be investigated numerically. Numerical integration of the ray equations (1) and (2) is simplified if the fact that ω is constant along a ray trajectory is used to eliminate k_r from these equations. This gives a system of three coupled equations in z, k_z, and r

$$\frac{dz}{dt} = \frac{c^2}{\omega}k_z, \tag{6a}$$

$$\frac{dk_z}{dt} = -\frac{\omega}{c}\frac{\partial c}{\partial z}, \tag{6b}$$

and

$$\frac{dr}{dt} = \frac{c^2}{\omega}\left(\frac{\omega^2}{c^2} - k_z^2\right)^{1/2}. \tag{6c}$$

Rather than presenting numerical results based on the solutions to these equations, we shall reduce them to a system of one-way ray equations. Numerical results based on the one-way ray equations will be presented in the following section.

Validity of the one-way ray equations requires that r increase monotonically along all ray trajectories of interest

$$\frac{dr}{dt} > 0. \tag{7}$$

Dividing Eqs. (1a), (1b), and (1d) by dr/dt (1c) gives

$$\frac{dz}{dr} = \frac{\partial \omega/\partial k_z}{\partial \omega/\partial k_r}, \tag{8a}$$

$$\frac{dk_z}{dr} = -\frac{\partial \omega/\partial z}{\partial \omega/\partial k_r}, \tag{8b}$$

and

$$\frac{dk_r}{dr} = -\frac{\partial \omega/\partial r}{\partial \omega/\partial k_r}. \tag{8c}$$

Because (4) gives k_r as a function of z, r, k_z, and ω (constant on a ray trajectory), Eq. (8c) is redundant and can be ignored. This leaves a pair of coupled ray equations (8a) and (8b). It follows from the dispersion relation (2) that the rhs of (8a) is equal to k_z/k_r. Thus, ray angle with respect to the horizontal

$$\theta = \tan^{-1}\left(\frac{dz}{dr}\right) = \tan^{-1}\left(\frac{k_z}{k_r}\right). \tag{9}$$

The one-way restriction (7) dictates that $|\theta| < \pi/2$. Equation (8b) can also be simplified. It follows from the condition

$$d\omega = \frac{\partial \omega}{\partial r}dr + \frac{\partial \omega}{\partial z}dz + \frac{\partial \omega}{\partial k_r}dk_r + \frac{\partial \omega}{\partial k_z}dk_z = 0 \tag{10}$$

that

$$\left(\frac{dk_r}{dz}\right)_{r,k_z,\omega} = -\frac{\partial \omega/\partial z}{\partial \omega/\partial k_r}, \tag{11}$$

where the subscripted variables on the left are held constant. Using Eqs. (4) and (11), the ray equations (8a) and (8b) can be written

$$\frac{dz}{dr} = \frac{\partial H}{\partial k_z} \tag{12a}$$

and

$$\frac{dk_z}{dr} = -\frac{\partial H}{\partial z}, \tag{12b}$$

where

$$H(z,k_z,r) = -k_r = -[\omega^2/c^2(z,r) - k_z^2]^{1/2}. \tag{13}$$

The frequency ω is, of course, regarded as a constant parameter. Equations (12) and (13) are the one-way elliptic ray equations. These equations define a Hamiltonian system with one degree of freedom: z, k_z, and r are the position, "momentum," and "time" variables, respectively, and H is the Hamiltonian.

The one-way elliptic ray equations (12) and (13) are integrable if there exists a constant of the motion $\chi(z,k_z,r)$ which satisfies

$$\frac{d\chi}{dr}=\frac{\partial\chi}{\partial z}\frac{dz}{dr}+\frac{\partial\chi}{\partial k_z}\frac{dk_z}{dr}+\frac{\partial\chi}{\partial r}=0. \tag{14}$$

In the range-independent problem, $c=c(z)$, $H(z,k_z)$ (13) is a constant of the motion: the first two terms on the rhs of (14) cancel and the third is identically zero. The ray equations are thus integrable in this case (as was shown previously). It follows that the ray motion is entirely regular. In the generic range-dependent problem, $c=c(z,r)$, however, no constant of the motion exists and the ray equations (12) are nonintegrable. Under such conditions, numerical techniques are used to investigate ray stochasticity.

The ω dependence in both forms of the ray equations that we have seen [(1) and (2); (12) and (13)] can be eliminated. For the two-way ray equations (1) and (2) this involves replacing k_i by the slowness $p_i=k_i/\omega$ and $\omega(\mathbf{x},\mathbf{k})$ by $H(\mathbf{x},\mathbf{p})=c(\mathbf{x})|\mathbf{p}|$. The rescaled Hamiltonian takes the constant value of one on all ray trajectories. This is a reflection of the fact that sound waves are nondispersive. (Recall, however, that the ray approximation is a high-frequency approximation.) For the one-way ray equations (12) and (13) we again replace k_i by $p_i=k_i/\omega$—and hence also $H=-k_r(z,k_z,r)$ by $H=-p_r(z,p_z,r)$. The comments made earlier regarding integrability of the ray equations are, of course, unchanged by this rescaling.

We now introduce the parabolic approximation. This is valid when ray angles with respect to the horizontal are small

$$|\theta|\ll 1. \tag{15}$$

Consistent with this approximation

$$|k_z|\ll k_r\approx k=\omega/c \tag{16}$$

and the Hamiltonian (13)

$$H(z,k_z,r)\approx H_{\mathrm{PE}}(z,k_z,r)=(1/2k)k_z^2-k. \tag{17}$$

In the ocean, sound-speed deviations from a constant c_0 are small. We set

$$c(z,r)=c_0[1+\epsilon\mu(z,r)], \tag{18}$$

where $\mu(z,r)$ is an order one quantity. Asymptotic balancing of the two terms in (17) requires that

$$\theta^2=O(\epsilon). \tag{19}$$

To this order we may set

$$\begin{aligned}H_{\mathrm{PE}}(z,k_z,r)&=(1/2k_0)k_z^2-k_0[1-\epsilon\mu(z,r)]\\&=(1/2k_0)k_z^2+k_0[(c(z,r)-c_0)/c_0]-k_0,\end{aligned} \tag{20}$$

where $k_0=\omega/c_0$. We may neglect the final constant term $-k_0$ in (20) as it has no influence on the ray trajectories which are defined by (20) and (12). Replacement of k_z by $p=k_z/k_0$ in these equations then yields the parabolic ray equations

$$\frac{dz}{dr}=\frac{\partial H}{\partial p}, \tag{21a}$$

$$\frac{dp}{dr}=-\frac{\partial H}{\partial z}, \tag{21b}$$

where

$$H(z,p,r)=\tfrac{1}{2}p^2+[c(z,r)-c_0]/c_0=\tfrac{1}{2}p^2+V(z,r). \tag{22}$$

Like the one-way elliptic ray equations, (12) and (13), these equations define a nonautonomous Hamiltonian system with one degree of freedom. As discussed above, they are integrable when the sound-speed structure is range independent and generally nonintegrable when the sound-speed structure is range dependent.

In this section we have discussed some of the connections between separability of a wave equation, integrability of the corresponding ray equations, and the type of motion, chaotic or regular, exhibited by ray trajectories. These connections are sufficiently important that some additional comments are warranted. First, there is a distinction between separable and integrable problems (see, e.g., Gutzwiller, 1990). While all separable problems are integrable (the separation constants are the required constants of the motion), nonseparability does not imply nonintegrability. In practice, however, the class of nonseparable but integrable problems is small and can be ignored. Generic Hamiltonian systems are nonintegrable (Marcus and Meyer, 1974). Second, nonintegrability of a set of ray equations is a necessary but not a sufficient condition for chaotic trajectories. The celebrated KAM theorem (see, e.g., Tabor, 1989) guarantees the existence of regular trajectories in certain classes of nonintegrable problems. This will be discussed in more detail in the following section.

II. POINCARÉ SECTIONS

In the remainder of this paper, we restrict our attention to sound-speed models with periodic range dependence, $c(z,r)=c(z,r+\lambda)$. All of the numerical results presented in this report are based on the use of a perturbed Munk (1974) sound-speed profile

$$\begin{aligned}c(z,r)=c_0[1+\epsilon(e^{-\eta}+\eta-1)\\+\delta(2z/B)e^{-2z/B}\cos(2\pi r/\lambda)],\end{aligned} \tag{23}$$

with depth z defined positive downwards. Here $\eta=2(z-z_{\mathrm{axis}})/B$ is a scaled depth coordinate, $z_{\mathrm{axis}}=1$ km is the sound channel axis depth, the depth scale $B=1$ km, the reference sound speed $c_0=1490$ m/s, and $\epsilon=0.0057$. The range-dependent perturbation has dimensionless magnitude δ and wavelength λ. The ocean surface and bottom are assumed to be flat, perfectly reflecting interfaces at depths $z=0$ and 4.5 km, respectively. This highly idealized class of model is useful to illustrate the fundamental differences between regular and chaotic trajectories. A similar ocean model has previously been used by Baer and Jacobson (1974, 1975) to investigate phase fluctuations of underwater acoustic signals.

For this class of problems, r can be defined modulo λ. Because the background sound-speed structure has the typical deep ocean waveguide character, both ray depth and ray angle are bounded. Ray trajectories, therefore, lie in a bounded three-dimensional space, $(z,\theta,r \bmod \lambda)$. The ray angle θ is defined relative to the horizontal and related to k_z or p through Eq. (9). If the system is integrable, a constant of the motion $\chi(z,\theta,r)$, as defined by Eq. (14), exists and all

trajectories lie on two-dimensional surfaces of constant χ in this three-dimensional space. In a bounded phase space, these surfaces are tori so ray trajectories lie on a set of nested tori. In generic range-dependent environments, the ray equations are nonintegrable and trajectories may be chaotic. With no surfaces of constant χ to restrict the motion, chaotic ray trajectories fill volumes in (z,θ,r).

To distinguish between these two types of behavior, one need only examine a two-dimensional slice of the three-dimensional space. This simple device—introduced by Poincaré—is commonly referred to as a surface of section or Poincaré section. On this slice, area and volume filling trajectories in (z,θ,r) lie on smooth curves and fill areas, respectively. These are referred to as regular and chaotic trajectories, respectively. For the class of problems considered here, Poincaré sections are constructed by stroboscopically viewing ray trajectories, $z(r)$, $\theta(r)$, at integer multiples of λ, $z(n\lambda)$, $\theta(n\lambda)$, $n = 0,1,2,\ldots$.

The ray equations were numerically integrated using fourth-order Runge–Kutta algorithms with double-precision arithmetic and a fixed range step of 100 m. The step size was chosen to be much smaller than length scales associated with the perturbations examined. Boundary reflections were treated by breaking the 100-m range step into pre- and post-reflection pieces. The length of the pre-reflection range step X m was found iteratively; the ray depth at reflection was required to lie within 10^{-12} m of the boundary. After changing the sign of p, the $(100 - X)$ m post-reflection range step was taken. Numerical accuracy was tested by forward- and back-tracing rays to see if their initial conditions could be recovered. For reasons to be discussed below, at long range this procedure works only for regular rays. For such rays, using a one-way range of 50 000 km, errors in reconstructed initial conditions were found to be less than 1 cm in depth and less than 1/10 of a millidegree in ray angle.

Figure 1 shows a comparison of Poincaré sections computed using the one-way elliptic [(12), (13)] and parabolic [(21), 22)] ray equations using the environment for which $\lambda = 10$ km and $\delta = 0.01$. Eleven rays are included in each plot with initial conditions $z(0) = 1$ km, $\theta(0) = 5°,6°,\ldots,$ 15°. For each initial condition, 500 points are plotted, one every λ, corresponding to a total computation range of 5000 km. Both plots show the same qualitative behavior. Near the center, rays remain regular with successive points falling on smooth curves. At larger launch angles, some rays form a series of closed curves ("islands") surrounded by speckled regions ("chaotic seas"). The formation of island structures is associated with a resonance between unperturbed ($\delta = 0$) rays and the range-dependent perturbation. Both forms of the ray equations produce five island structures for rays whose unperturbed ($\delta = 0$) wavelengths are 50 km. The five islands are associated with a 5:1 resonance between these rays and the 10-km perturbation. The same general regions (the speckled regions) are covered by chaotic rays in both figures, indicating that the same fundamental dynamics are predicted by the elliptic ray equations and the parabolic ray equations. The remainder of our numerical experiments will be conducted using the parabolic ray equations (21) and (22).

The main reason for making this choice is pedagogical. The purpose of this work is to illustrate the fundamental differences between sound ray behavior in range-indepen-

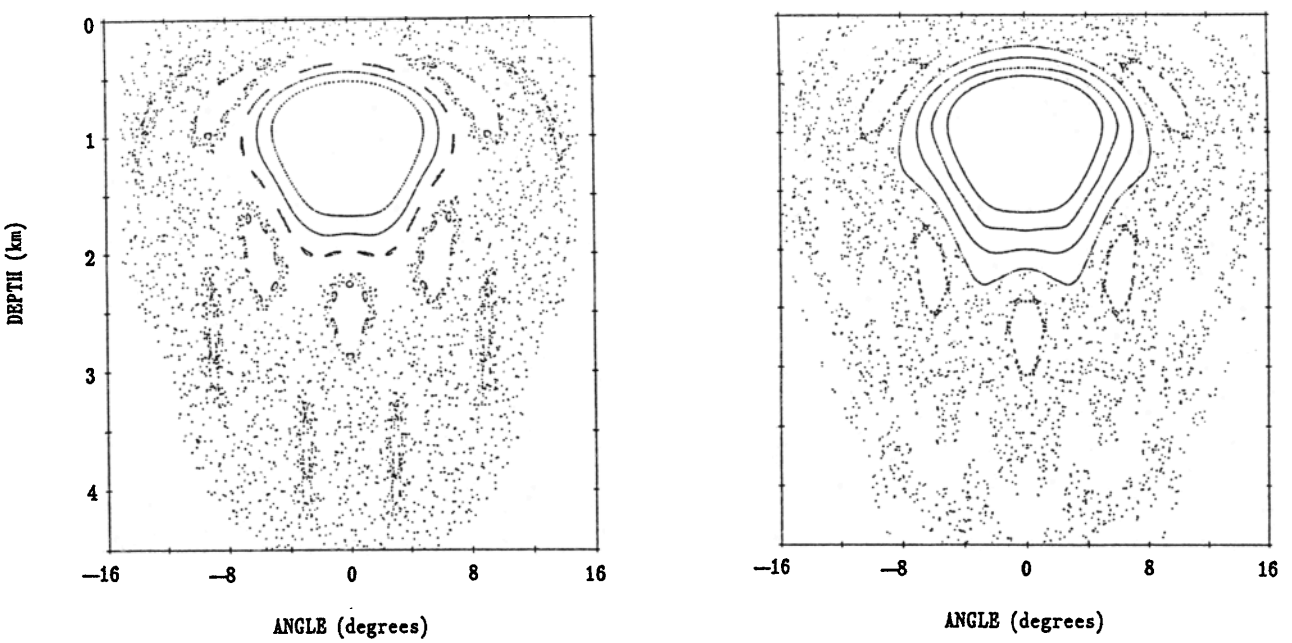

FIG. 1. Poincaré sections computed for rays with initial conditions $z(0) = 1$ km, $\theta(0) = 5°,6°,\ldots,15°$, in the model environment for which $\lambda = 10$ km, $\delta = 0.01$. (left) calculation using elliptic ray equations (12) and (13); (right) calculation using parabolic ray equations (21) and (22).

dent and range-dependent environments. The parabolic ray equations are best suited to this task inasmuch as they are the simplest set of equations which illustrate this difference. The minor distortion associated with the parabolic approximation is not important in this study. A second reason for our use of the parabolic ray equations is our anticipation that this ray chaos work will be followed by extensive studies of "wave chaos" whose purpose is to understand the manifestations of chaotic ray trajectories on the corresponding finite frequency wave fields. Wave chaos studies unavoidably involve generating solutions to a linear wave equation. In range-dependent environments, solutions to the parabolic wave equation (Tappert, 1977) are easily generated numerically; solutions to the Helmholtz equation are not.

Figure 2 shows a set of Poincaré sections computed for the environment for which $\lambda = 10$ km as the range-dependent perturbation strength δ is increased from 0 to 0.01. In the first plot, $\delta = 0$ and all rays fall on smooth, embedded curves, each such curve being a slice of a torus in (z,θ,r). For nonzero perturbation strengths, some tori remain stable while others break up into stable islands or chaotic seas. The fraction of phase space which is filled with chaotic rays is seen to increase as the range-dependent perturbation strength increases. In addition to the 5:1 resonance structure observed when $\delta = 0.01$, a chain of nine islands is seen when $\delta = 0.005$. This is due to a 9:2 resonance corresponding to an unperturbed ray wavelength of 45 km. Upon closer examination, each island is found to consist of an even smaller chain of islands separated by chaotic regions. When the perturbation parameter is then increased to $\delta = 0.01$, this stable structure breaks down but the five-island structure persists.

Figure 3 shows a set of Poincaré sections for six choices of perturbation wavelength λ. As was the case previously, the formation of multiple island structures is associated with resonances between the unperturbed rays and the periodic perturbation. For example, the three-island structure seen in the $\lambda = 15$-km section is due to a 3:1 resonance between rays with unperturbed wavelengths near 45 km and the perturbation. For the larger values of λ the single island structures are due to subharmonic resonances, e.g., 1:3 for $\lambda = 150$ km. Note that, in this figure, the perturbation strength δ is larger for the longer wavelength perturbations than for the shorter wavelength perturbations. The reason for this choice is that little or no chaos is observed for $\lambda \geqslant 150$ km for the same value of perturbation strength, $\delta = 0.01$, used to produce the plots for $\lambda \leqslant 50$ km. This behavior is probably due to the presence of an adiabatic invariant under those circumstances in which the perturbation is weak and slowly varying.

The coexistence of regular and chaotic trajectories seen in Figs. 1–3 is predicted by the celebrated KAM theorem and is commonly observed in almost-integrable Hamiltonian systems (see, e.g., Tabor, 1989). Loosely speaking, the KAM theorem states that some of the invariant tori of a bounded integrable Hamiltonian system survive (but may be distorted) under the influence of certain classes of sufficiently small perturbations to the Hamiltonian. The periodically range-dependent perturbations considered here are of the type for which the KAM theorem applies. Although realistic range-dependent ocean structure is not periodic, the KAM theorem is important inasmuch as it states that regular ray motion may persist under conditions in which the ray equations are nonintegrable.

While the construction of Poincaré sections for periodically range-dependent sound-speed structures simplifies the task of distinguishing regular rays from chaotic rays, this procedure cannot be applied to more general range dependence. In constrast, the techniques described in the two sections that follow can be applied to ray motion in generally range-dependent environments.

III. POWER SPECTRA

When a transformation of the canonical phase space variables is made to action-angle variables (see, e.g., Gold-

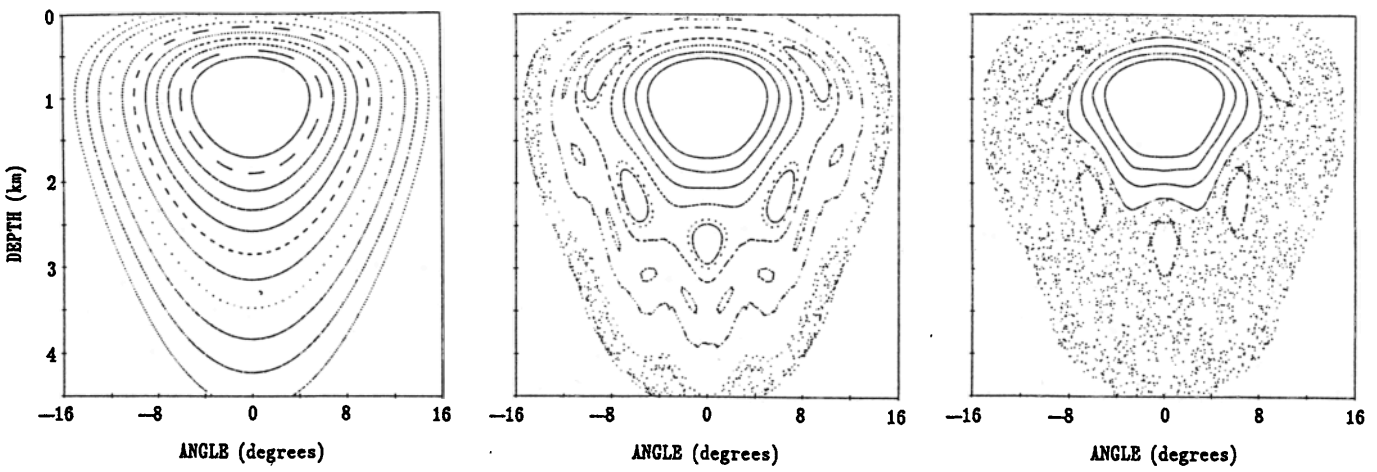

FIG. 2. Poincaré sections for rays with initial conditions $z(0) = 1$ km, $\theta(0) = 5°,6°,...,15°$, in the family of model environments for which $\lambda = 10$ km; (left) $\delta = 0$; (center) $\delta = 0.005$; (right) $\delta = 0.01$.

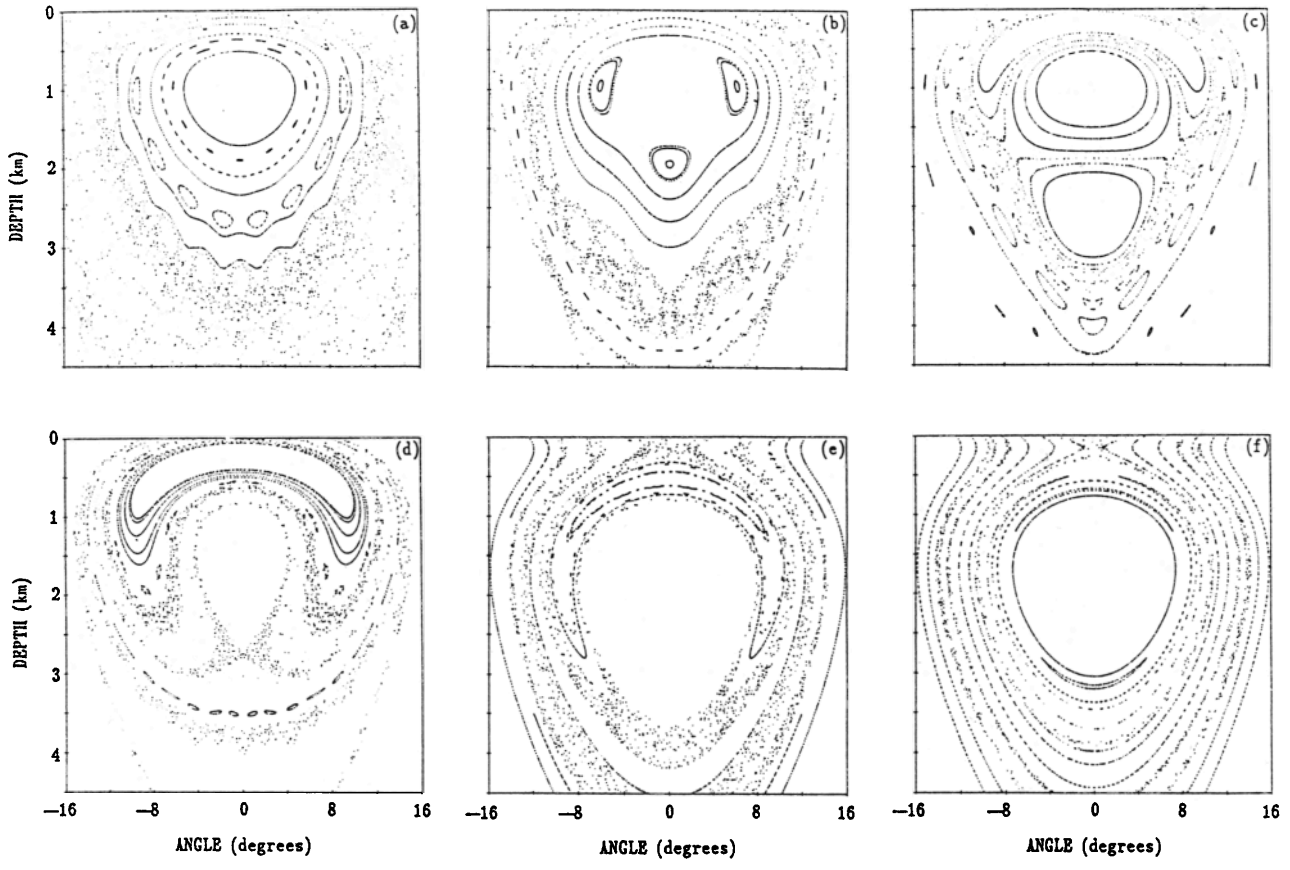

FIG. 3. Poincaré sections for rays with initial conditions $z(0) = 1$ km, $\theta(0) = 5°,6°,...,15°$, in the model environments for which: (a) $\lambda = 5$ km, $\delta = 0.01$; (b) $\lambda = 15$ km, $\delta = 0.01$; (c) $\lambda = 25$ km, $\delta = 0.01$; (d) $\lambda = 50$ km, $\delta = 0.01$, (e) $\lambda = 150$ km, $\delta = 0.05$; (f) $\lambda = 250$ km; $\delta = 0.05$.

stein, 1980), the motion in bounded integrable Hamiltonian systems is seen to be periodic. This is obvious geometrically as the trajectories lie on tori. Because the transformation between action-angle variables and $z(r)$, $p(r)$ is generally nonlinear, harmonics may be present in spectra of the latter. These spectra remain discrete, however. In contrast, chaotic trajectories are characterized by broadband, apparently noisy spectra. This difference is consistent with the expectation (to be quantified in the following section) that the large r behavior of regular rays is predictable while that of chaotic rays is not.

To illustrate this difference, spectra of three rays $z(r)$ are plotted in Fig. 4. The first ray was computed using a range-independent environment $\delta = 0$. The distinct peaks in the spectrum indicate that the ray is regular. When the perturbation strength is increased to $\delta = 0.005$, the spectrum is seen to exhibit more structure. The final plot, showing a highly structured spectrum when $\delta = 0.01$, suggests the presence of chaos. This is consistent with the chaotic behavior of this ray as indicated in the final Poincaré section of Fig. 2.

Although the calculation of power spectra and the construction of Poincaré sections are insightful, both tools suffer from the shortcoming of being unable to provide a quantitative measure of how chaotic a ray trajectory is. The Lyapunov exponent introduced in the next section is such a measure.

IV. LYAPUNOV EXPONENTS

Asymptotically, chaotic and regular trajectories diverge exponentially and according to a power law, respectively, from their neighbors. A quantitative measure of this difference is the Lyapunov exponent

$$\nu = \lim_{r\to\infty} \lim_{d(0)\to 0} \frac{1}{r} \ln \frac{d(r)}{d(0)}. \tag{24}$$

Here, $d(r)$ is the separation between neighboring trajectories in phase space. Chaotic and regular trajectories have $\nu > 0$ and $\nu = 0$, respectively. In the remainder of this section we discuss the calculation of Lyapunov exponents and then consider some of the implications of chaotic motion.

The ray separation $d(r)$, which appears in the definition of the Lyapunov exponent (24), is a measure of separation in phase space. It is tempting to use a pair of neighboring rays to compute $d(r)$ as

$$d(r) = \{[z_1(r) - z_2(r)]^2 + [p_1(r) - p_2(r)]^2\}^{1/2}. \tag{25}$$

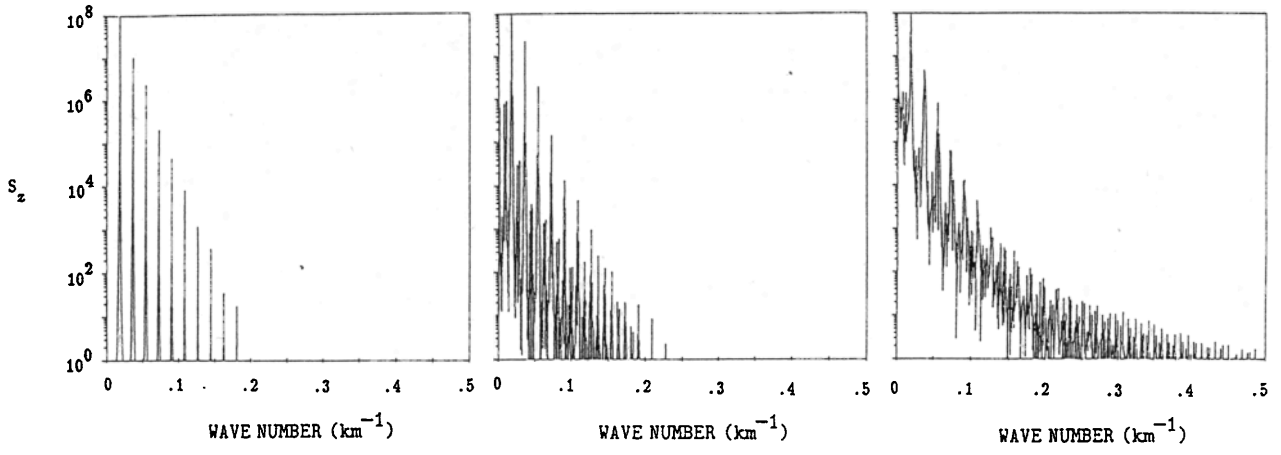

FIG. 4. Power spectra of ray trajectories $z(r)$ whose initial conditions are $z(0) = 1$ km, $\theta(0) = 12°$, in the family of model environments for which $\lambda = 10$ km: (left) $\delta = 0$; (center) $\delta = 0.005$; (right) $\delta = 0.01$.

There are two problems with this approach. To understand the first problem, consider the evolution in range of a continuum of initial conditions consisting of a finite length line segment in phase space (z,p). (Such behavior is considered in more detail in Sec. V.) Such a segment will in general grow and develop more structure as r increases. At sufficiently long range the separation between endpoints of the segment [as in Eq. (25)] will significantly underestimate the rate at which infinitesimal elements grow [as in Eq. (24)]. This problem is sometimes referred to as "saturation." The second problem associated with the use of Eq. (25) is that this equation requires that two numbers with different units $z(r)$ and $p(r)$ be added. This problem can be avoided by nondimensionalizing the ray equations. The scales chosen to nondimensionalize the ray equations are not unique, however.

The first problem encountered in determining ν, saturation, can be eliminated by defining the variational parameters δz and δp. The variational equations follow from the ray equations (21) and (22):

$$\frac{d}{dr}\begin{bmatrix}\delta z\\ \delta p\end{bmatrix} = \begin{bmatrix} H_{zp} & H_{pp}\\ -H_{zz} & -H_{pz}\end{bmatrix}\begin{bmatrix}\delta z\\ \delta p\end{bmatrix} = \begin{bmatrix} 0 & 1\\ -V_{zz} & 0\end{bmatrix}\begin{bmatrix}\delta z\\ \delta p\end{bmatrix}. \tag{26}$$

The variational equations (26) and the ray equations (21) define a system of four coupled equations which can be integrated to give $z(r), p(r), \delta z(r)$, and $\delta p(r)$ given a knowledge of their initial conditions. These equations describe how small elements $\delta z\, \delta p$ of phase space are stretched as the ray trajectory evolves. Given $\delta z(r)$ and $\delta p(r)$, we may set $d(r) = [\delta z(r)^2 + \delta p(r)^2]^{1/2}$. More generally, any norm of the vector $[\delta z(r), \delta p(r)]$ can be used to define $d(r)$. This procedure guarantees that the requirement $d(0) \to 0$ is satisfied because the variational parameters are, by definition, infinitesimal quantities. Nondimensionalization of z and p allows the variational quantities δz and δp to be combined. The result of such a calculation will be shown, below, to produce the same estimate of ν as the following method which avoids the necessity of using dimensionless variables.

The variational equations can be combined to give

$$\frac{d^2(\delta z)}{dr^2} + \frac{\partial^2 V}{\partial z^2}\delta z = 0. \tag{27}$$

There are two fundamental solutions to (27), $\delta z_1(r)$, and $\delta z_2(r)$, which are assumed to satisfy

$$\delta z_1(0) = 1, \quad \frac{d(\delta z_1)}{dr}(0) = 0,$$
$$\delta z_2(0) = 0, \quad \frac{d(\delta z_2)}{dr}(0) = 1. \tag{28}$$

The Wronskian of these two solutions is unity

$$W(r) = W(0)$$
$$= \delta z_1(0)\frac{d(\delta z_2)}{dr}(0) - \delta z_2(0)\frac{d(\delta z_1)}{dr}(0) = 1. \tag{29}$$

[Constancy of the Wronskian follows from the fact that the coefficient of $(d/dr)(\delta z)$ in (27) is zero.]

Solutions of the variational equations $\delta z_1(r)$ and $\delta z_2(r)$ can be combined to form a pair of equations which relate $dz(r)$ and $dp(r)$ to $dz(0)$ and $dp(0)$:

$$\begin{bmatrix}dz(r)\\ dp(r)\end{bmatrix} = \begin{bmatrix}\dfrac{dz}{dz(0)} & \dfrac{dz}{dp(0)}\\ \dfrac{dp}{dz(0)} & \dfrac{dp}{dp(0)}\end{bmatrix}\begin{bmatrix}dz(0)\\ dp(0)\end{bmatrix} = J(r)\begin{bmatrix}dz(0)\\ dp(0)\end{bmatrix}. \tag{30}$$

Here the Jacobi matrix is

$$J(r) = \begin{bmatrix}\delta z_1(r) & \delta z_2(r)\\ \dfrac{d}{dr}\delta z_1(r) & \dfrac{d}{dr}\delta z_2(r)\end{bmatrix} = \begin{bmatrix}\delta z_1(r) & \delta z_2(r)\\ \delta p_1(r) & \delta p_2(r)\end{bmatrix}, \tag{31}$$

where the second equality follows from Eqs. (21) and (22). Equation (29) guarantees that the Jacobi matrix has determinant 1.

Assume that the eigenvalues and eigenvectors of $J(r)$, $\lambda_i(r)$, and $\mathbf{u}_i(r)$, $i=1,2$, are ordered such that $|\lambda_1(r)| \geqslant |\lambda_2(r)|$. Because $\det J(r) = 1$, $\lambda_1(r)\lambda_2(r) = 1$. The solution to (30) is a linear combination of $\lambda_i(r)\mathbf{u}_i(r)$. Under chaotic conditions

$$|\lambda_1(r)| \sim e^{\nu r} \quad \text{and} \quad |\lambda_2(r)| \sim e^{-\nu r} \quad \text{as} \quad r \to \infty. \tag{32}$$

The Lyapunov exponent can be defined as

$$\nu \equiv \lim_{r\to\infty} (1/r) \ln |\lambda_1(r)|. \tag{33}$$

Strictly speaking, ν is the larger of two Lyapunov exponents whose sum is zero. These exponents describe the simultaneous stretching and contracting of phase space elements.

Figure 5 shows a comparison of three methods to estimate the (largest) Lyapunov exponent: (1) Eq. (24) using (25) to form $d(r)$ with $d(0) = 10^{-12}$; (2) Eq. (24) using the solution to the variational equations (26) with $[\delta z(0), \delta p(0)] = (0,1)$ to form $d(r)$; and (3) Eq. (33). The three plots are nearly indistinguishable, giving similar estimates for ν—about $(200 \text{ km})^{-1}$. Methods (2) and (3) require integration of the variational equations, necessitating that $c(z,r)$ be specified analytically. Method (3) requires the simultaneous calculation of two sets of variational equations. Method (2) requires one set and method (1) requires none (only trajectory components are needed).

The quantitative agreement of the three Lyapunov exponent estimates is expected. Growth of the separation in both z and p should closely approximate growth of the variational quantities δz and δp, provided these separations remain small at all ranges of interest. This was the case for the results shown in Fig. 5. The agreement between estimates of ν computed using (24) and (33) is also not surprising. Under chaotic conditions small elements of phase space $\delta z\, \delta p$ are simultaneously being stretched and compressed at an exponential rate. Generically, the separation between pairs of points will be dominated by the exponential stretching. This behavior is robust: separation may be measured in z, p, or some combination thereof (after nondimensionalization). This is consistent with the results shown in Fig. 5.

As a practical matter we recommend the use of Eq. (24) to estimate ν with $d(r) = |\delta z(r)| + |\delta p(r)|$, and with δz and δp computed using the variational equations (26). This necessitates writing the ray and variational equations in nondimensional form. The choice of initial conditions $\delta z(0)$ and $\delta p(0)$ is not important. This technique eliminates potential problems associated with saturation [using (25)] and requires less computation than use of the Jacobi matrix (33) to estimate ν. To avoid overflow problems δz and δp must be rescaled occasionally. In addition, the sign of δp (or δz, but not both) must be changed upon reflection to guarantee that the variational parameter estimates of $d(r)$ agree with the small $d(0)$ ray separation estimates. This condition also has the effect of reversing the sign of the Wronskian upon reflection. It should be noted that this situation occurs only for large initial launch angle, typical $\theta(0) \gtrsim 12°$. Rays with smaller initial launch angles did not interact with either boundary.

The procedure outlined above was used to produce the Lyapunov exponent estimation calculations seen in Fig. 6. These plots show the onset of chaos using a set of rays with the same initial conditions as the strength of the range-dependent perturbation δ increases. The same set of rays were used to produce Fig. 4. For the final plot, corresponding to $\delta = 0.01$, ν appears to be approximately $(170 \text{ km})^{-1}$.

The exponential divergence of neighboring ray trajectories under chaotic conditions leads unavoidably to the conclusion that under such conditions deterministic predictions using ray theory are not possible at long ranges ($\nu r \gg 1$). To understand why, consider the problem of finding the eigenrays connecting a source and receiver at fixed depths as the range between them increases. To find eigenrays, rays leaving the source at many launch angles $\theta(0)$ might be traced out to the receiver range r. By iteratively searching in launch angle, eigenrays, those rays which fall within some specified depth tolerance dz of the receiver, can be found. Under chaotic conditions $d\theta(0)/dz$ grows, on average, like $10^{\nu' r}$. Here $\nu' = \nu/\ln(10)$ is the Lyapunov exponent expressed in base 10. Suppose, for instance, that the initial ray angle must be

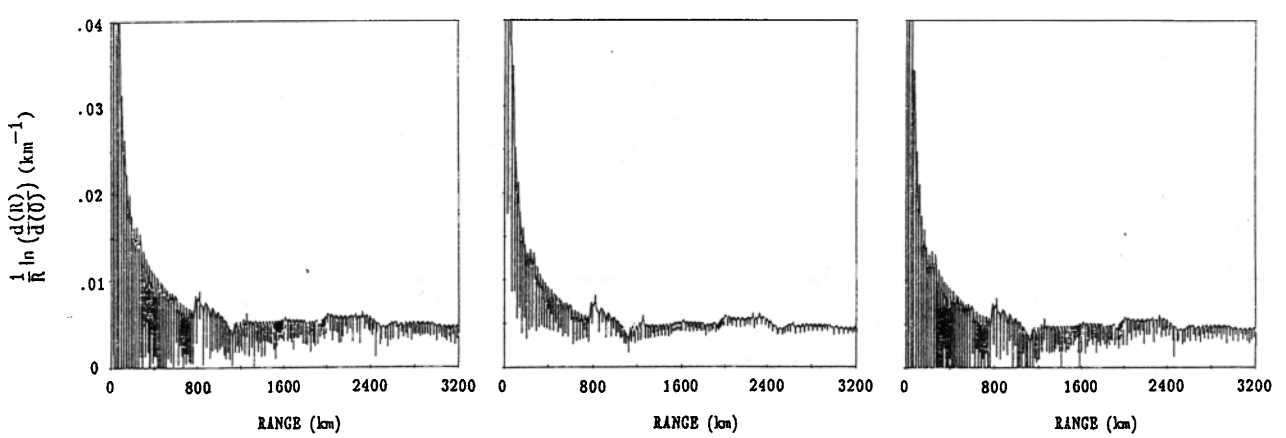

FIG. 5. A comparison of three Lyapunov exponent estimation methods for the same ray; (left) Eqs. (24) and (25) with $d(0) = 10^{-12}$; (center) Eqs. (24) and (26) with $[\delta z(0), \delta p(0)] = (0,1)$; (right) Eq. (33).

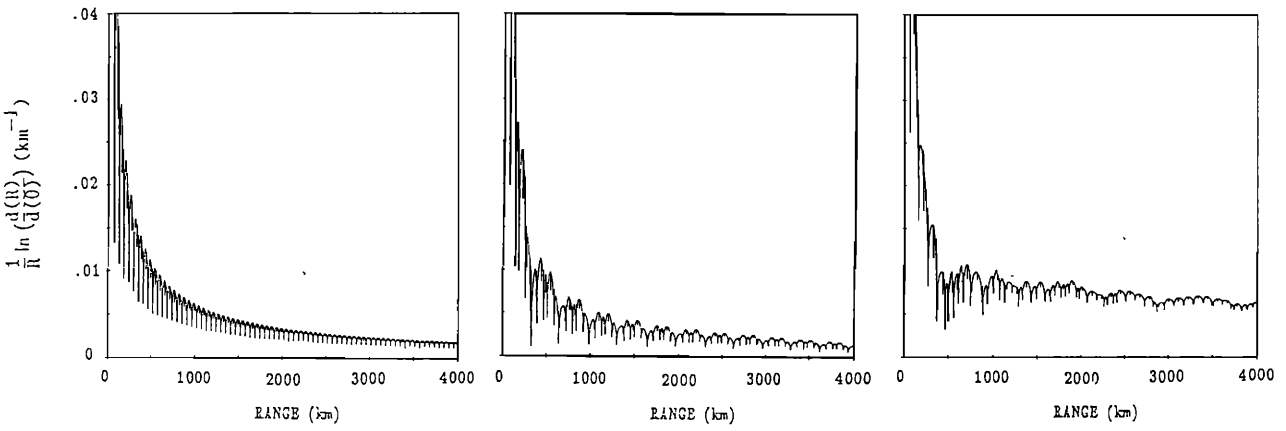

FIG. 6. Lyapunov exponent estimates for a ray with initial conditions $z(0) = 1$ km, $\theta(0) = 12°$ in the family of model environments for which $\lambda = 10$ km: (left) $\delta = 0$; (center) $\delta = 0.005$; (right) $\delta = 0.01$.

specified with 5-digit accuracy to satisfy the depth tolerance criterion at $r = 100$ km and $\nu' = (100 \text{ km})^{-1}$. Then at 200 km, 300 km, 400 km, ... 6-, 7-, 8-, ... digit accuracy in the specification of $\theta(0)$ is required. At ranges beyond a few hundreds of km this condition cannot be met as the required machine precision will exceed that which is available. We may thus identify ν^{-1} as a "predictability horizon"—an order magnitude estimate of the range over which deterministic predictions are feasible. At ranges significantly in excess of ν^{-1}, computed ray trajectories will be sensitive to machine-dependent round-off algorithms. Such rays will have effectively forgotten their initial conditions.

This extreme sensitivity to initial conditions also carries over to environmental conditions. This becomes clear when the ray equations are written in dimensionless form. In terms of $z^0 = 2z/B$, $\eta^0 = z^0 - z^0_{\text{axis}}$ and $r^0 = 2r/B$ the ray equations (21) and (22) with sound speed given by (23) are

$$\frac{dz^0}{dr^0} = p, \tag{34a}$$

$$\frac{dp}{dr^0} = \epsilon(e^{-\eta^0} - 1) + \delta(z^0 - 1)e^{-z^0}\cos[(B/\lambda)\pi r^0 + \alpha]. \tag{34b}$$

If the environmental parameter B is perturbed, the dimensionless depth variable z^0 will also be perturbed. Because solutions to Eqs. (34) are known to exhibit chaotic behavior, the corresponding ray trajectories will diverge exponentially from each other (in the scaled range variable). The same argument applies to more complicated environments: the nondimensional variables will depend on environmental parameters, which, when perturbed, will cause a perturbation to the nondimensional initial conditions. Thus extreme sensitivity applies to both initial and environmental conditions. The cause of the limited ability to predict ray trajectories is then the limited experimental ability to measure accurate values of the input parameters—both initial and environmental conditions. The finite predictability horizons we have found are a direct consequence of the fundamental limitation of any experimental measurement of input conditions.

V. EXPONENTIAL PROLIFERATION OF MULTIPATHS

The exponential stretching of phase space elements under chaotic conditions is illustrated in Fig. 7. This set of plots shows the evolution in range of a fan of rays corresponding to the initial conditions $z(0) = 2.5$ km, $2° \leqslant \theta(0) \leqslant 6°$ in the environment described by (23) with $\lambda = 10$ km and $\delta = 0.01$. The Poincaré sections shown in Figs. 1 and 2 suggest that the rays in this band are predominantly chaotic. Assuming that these rays have the same Lyapunov exponent ν, the length of the segment should grow, on average, like $\exp(\nu r)$. This is consistent with the observed behavior. Figure 7 also suggests that phase space elements are being compressed at an exponential rate in the direction transverse to the stretching direction. The evolution of curves in phase space under regular and chaotic conditions has previously been considered by Berry *et al.* (1979).

One important consequence of the exponential stretching of the curve shown in Fig. 7 under chaotic conditions is that, under such conditions, the number of eigenrays grows exponentially, on average, as a function of range. Eigenrays correspond to the intersection of the plotted curve with a horizontal line at the receiver depth. Because the length of the phase space curve grows exponentially, on average, the number of intersections of such a curve with a horizontal line will also grow, on average, at the same exponential rate. Meanwhile, eigenray intensity must decay on average, at the same exponential rate. This is a consequence of energy conservation.

VI. SUMMARY

In this paper we have considered sound ray dynamics in range-dependent ocean environments. In such an environment, the acoustic ray equations, which have Hamiltonian

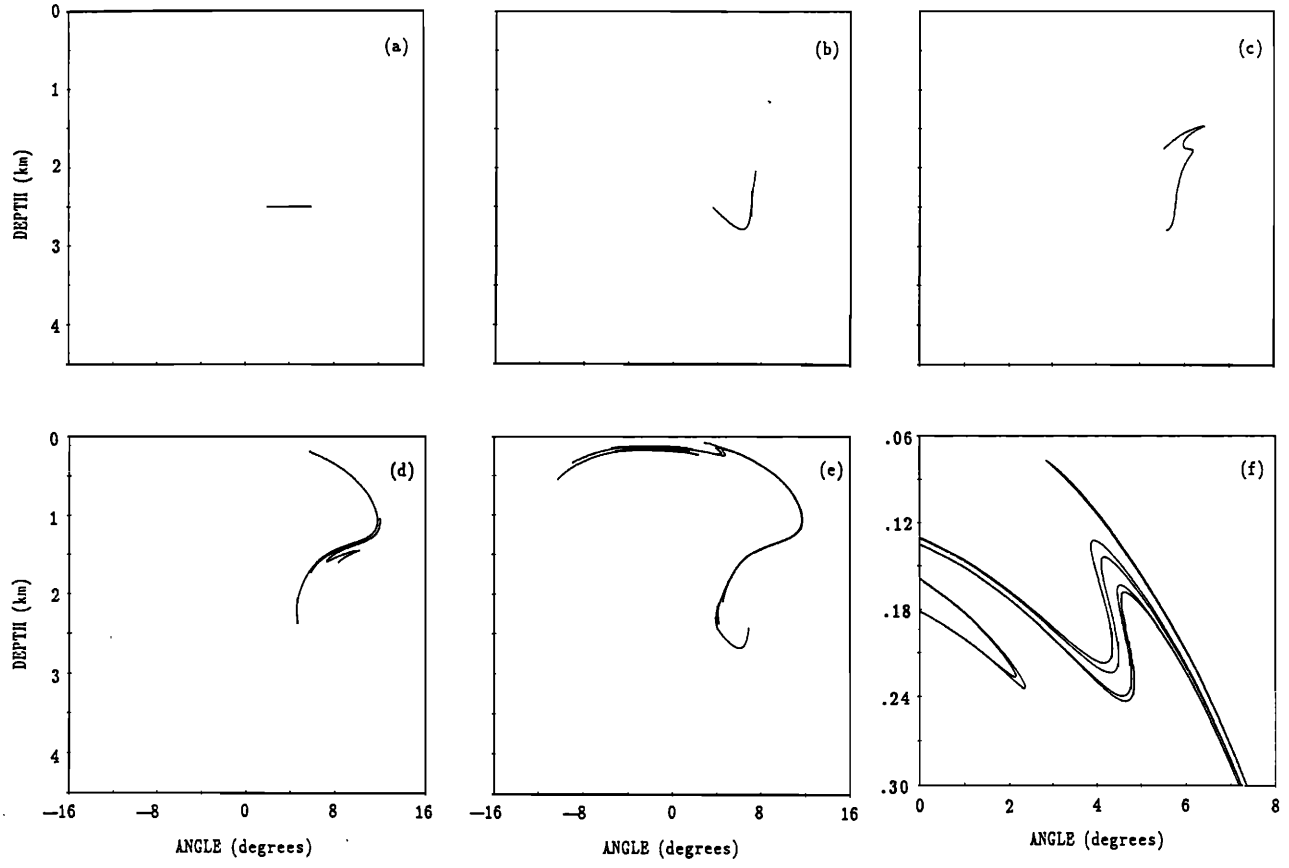

FIG. 7. Evolution of a fan of rays in phase space as a function of range in the model environment for which $\lambda = 10$ km, $\delta = 0.01$: (a) $r = 0$ km; (b) $r = 100$ km; (c) $r = 200$ km; (d) $r = 300$ km; (e) $r = 400$ km; (f) $r = 400$ km (expanded scale).

form, are expected to be nonintegrable and admit chaotic solutions. This expectation was confirmed numerically using simple periodically range-dependent ocean models. Solutions of the elliptic ray equations and the parabolic ray equations were shown to exhibit the same qualitative behavior. To distinguish between regular and chaotic behavior, Poincaré sections were constructed, power spectra were computed, and Lyapunov exponents were estimated. The three types of calculation were shown to give consistent pictures of the underlying ray dynamics. Different methods to estimate Lyapunov exponents gave similar results. It was argued that under chaotic conditions deterministic ray predictions are feasible only within the first few e-folding distances (inverse Lyapunov exponent). Thus ν^{-1} can be interpreted as an order of magnitude estimate of a ray "predictability horizon." Under chaotic conditions the number of eigenrays grows exponentially in range while average eigenray intensity decays exponentially.

The main purposes of this work were to introduce the concept of ray chaos in underwater acoustics and to point out the fundamental differences between sound ray propagation in range-independent and generic range-dependent environments. Because all of the numerical work presented was based on the unrealistic assumption of periodic range dependence, the reported quantitative measures of ray chaos (Lyapunov exponents) should not be considered as representative oceanographic values. It should be clear that both the oceanographic and the acoustic assumptions of the work reported here need to be made more realistic.

In a companion paper (Smith *et al.*, 1992), ray chaos in a more realistic class of ocean models is considered. The range-dependent perturbation is modelled as a randomly phased superposition of several baroclinic modes of the linearized quasigeostrophic potential vorticity equation. The purpose of that work is to determine whether sound rays in realistic models of mesoscale ocean structure are chaotic and to quantify this effect via the calculation of Lyapunov exponents. That work leads to an improved understanding of the computational limitations of ray theory in realistic ocean models.

More important than understanding these computational limitations, however, is understanding the extent to which chaotic ray behavior is felt in finite frequency wave fields. Although the related quantum mechanical problem has been extensively studied (see, e.g., Berry, 1987) this topic remains enigmatic. Numerical work on "wave chaos" in underwater acoustics (Goñi, 1991) suggests that the lack of predictability of chaotic ray trajectories does not carry over to finite frequency wave fields in spite of the fact that these wave fields may have a random appearance. The manner in

which the chaotic high-frequency limit of the linear acoustic wave equation is approached is currently not well understood.

ACKNOWLEDGMENTS

We thank Dr. D. Palmer, Dr. H. Bezdek, Dr. A. Griffa, and Dr. J. Willemsen for the benefit of our discussions on chaos. This work was suported by the Office of Naval Research and the National Science Foundation.

Abdullaev, S. S., and Zaslavskii, G. M. (**1989**). "Fractals and ray dynamics in a longitudinally inhomogeneous medium," Sov. Phys Acoust. **34**, 334–336.

Baer, R. N., and Jacobson, M. J. (**1974**). "Effect of a Rossby wave on the phase of an underwater acoustic signal," J. Acoust. Soc. Am. **56**, 809–816.

Baer, R. N., and Jacobson, M. J. (**1975**). "SOFAR transmission fluctuations produced by a Rossby wave," J. Acoust. Soc. Am. **57**, 569–576.

Berry, M. V. (**1977**). "Regular and irregular motion," in *Topics in Nonlinear Dynamics. A Tribute to Sir Edward Ballard*, edited by Siebe Jorna (American Institute of Physics, New York), pp. 16–120.

Berry, M. V., Balazs, N. L., Tabor, M., and Voros, A. (**1979**). "Quantum Maps," Ann. Phys. **122**, 26–63.

Berry, M. V. (**1987**). "Quantum chaology," Proc. R. Soc. London Ser. A **413**, 183–198.

Brown, M. G., Tappert, F. D., and Goñi, G. (**1991a**). "An investigation of sound ray dynamics in the ocean volume using an area preserving mapping," Wave Motion **14**, 93–99.

Brown, M. G., Tappert, F. D., Goñi, G., and Smith, K. B. (**1991b**). "Chaos in underwater acoustics," in *Ocean Variability and Acoustic Propagation*, edited by J. Potter and A. Warn-Varnas (Kluwer Academic, Dordrecht), pp. 139–160.

Foreman, T. L. (**1983**). "Ray modeling method for range dependent ocean environments," ARL Tech. Rep. No. 83–41, Applied Research Laboratories, The University of Texas at Austin, Austin, TX.

Goldstein, H. (**1980**). *Classical Mechanics* (Addison-Wesley, Reading, MA).

Goñi, G. J. (**1991**). "Ray and wave chaos in underwater acoustics," Ph. D. dissertation, University of Miami.

Gutzwiller, M. C. (**1990**). *Chaos in Classical and Quantum Mechanics* (Springer-Verlag, New York).

Henon, M. (**1983**). " Numerical exploration of Hamiltonian systems," in *Chaotic Behavior of Deterministic Systems (Les Houches Lectures 36)*, edited by G. Iooss, R. G. H. Helleman, and R. Stora (North-Holland, Amsterdam), pp. 53–170.

Jones, R. M., Riley, J. P., and Georges, T. M. (**1986**). "HARPO: A versatile three-dimensional Hamiltonian ray-tracing program for acoustic waves in an ocean with irregular bottom," Wave Propagation Laboratory, Boulder, CO.

Landau, L. D., and Lifshitz, E. M. (**1959**). *Fluid Mechanics* (Pergamon, New York), pp. 256–259.

Lichtenberg, A. J., and Lieberman, M. A. (**1983**). *Regular and Stochastic Motion* (Springer-Verlag, New York).

Marcus, L., and Meyer, K. R. (**1974**). *General Hamiltonian Systems are Neither Integrable nor Ergodic*, Mem. Am. Math. Soc. No. 144 (Am. Math. Soc., Providence, RI).

Munk, W. H. (**1974**). "Sound channel in an exponentially stratified ocean with application to SOFAR." J. Acoust. Soc. Am. **55**, 220–226.

Palmer, D. R., Brown, M. G., Tappert, F. D., and Bezdek, H. F. (**1988**). "Classical chaos in nonseparable wave propagation problems," Geophys. Res. Lett. **15**, 569–572.

Smith, K. B., Brown, M. G., and Tappert, F. D. (**1992**). "Acoustic ray chaos induced by mesoscale ocean structure," J. Acoust. Soc. Am. **91**, 1950–1959.

Tabor, M. (**1989**). *Chaos and Integrability in Nonlinear Dynamics* (Wiley–Interscience, New York).

Tappert, F. D. (**1977**). "The parabolic approximation method," in Lecture Notes in Physics, Vol. 70, *Wave Propagation and Underwater Acoustics*, edited by J. B. Keller and J. S. Papadakis (Springer-Verlag, New York), pp. 224–287.

Tappert, F. D., Brown, M. G., and Goñi, G. (**1991**). "Weak chaos in an area-preserving mapping for sound ray propagation," Phys. Lett. A **153**, 181–185.